Water Air Soil Pollut (2021) 232: 294
https://doi.org/10.1007/s11270-021-05229-6

Dynamics and Treatability of Heavy Metals in Pig Farm Effluent Wastewater by Using UiO-66 and UiO-66-NH_2 Nanomaterials as Adsorbents

Leiping Wang · Xiaorong Dai · Zun Man · Jianrong Li · Yifeng Jiang · Dezhao Liu · Hang Xiao · Sanjay Shah

Received: 5 March 2021 / Accepted: 13 June 2021 / Published online: 6 July 2021

Abstract Concentrated pig production is a major source of environmental pollution. Metal–organic frameworks (MOFs) show potential for reducing heavy metal pollution. Two zirconium-based octahedral MOFs, UiO-66 and UiO-66-NH_2, were prepared by solvothermal method and were characterized by XRD, SEM, FT-IR, and BET. The adsorption capacity, treatability, and reusability of the adsorbents were tested in batch experiments. The optimum adsorbent dosage was 4 g/L, and the maximum removal rates at room temperature of chromium (Cr), manganese (Mn), iron (Fe), nickel (Ni), and Arsenic (As) on UiO-66 were 76.93%, 93.73%, 88.81%, 83.30%, and 86.11%, respectively. In the kinetic experiments, the adsorption process achieved equilibrium within 90 min and generally conformed to the quasi-second kinetics model. The results demonstrated that UiO-66 and UiO-66-NH_2 can be used over a wide range of pH for removal of most HMs on a large scale. Meanwhile, the adsorbents maintained excellent adsorption capacity after at least 3 cycles. Overall, UiO-66 and UiO-66-NH_2 have a high potential for practical application on the recovery of heavy metals in the complex wastewater from animal farms.

Keywords Animal wastewater · Heavy metals · Zr-MOFs · Absorption and reduction

L. Wang · Y. Jiang (✉)
College of Environment, Zhejiang University of Technology (ZJUT), Hangzhou 310014, China
e-mail: jyf@zjut.edu.cn

L. Wang · X. Dai (✉) · J. Li · H. Xiao
Zhejiang Key Laboratory of Urban Environmental Processes and Pollution Control, Ningbo Urban Environment Observation and Research Station, Chinese Academy of Sciences, Ningbo 315800, China
e-mail: xrdai@iue.ac.cn

L. Wang · X. Dai · J. Li · H. Xiao
Center for Excellence in Regional Atmospheric Environment & Key Laboratory of Urban Environment and Health, Institute of Urban Environment, Chinese Academy of Sciences, Xiamen 361021, China

Z. Man · D. Liu
College of Biosystems Engineering and Food Science, Zhejiang University, Hangzhou 310058, China

S. Shah
Department of Biological and Agricultural Engineering, North Carolina State University, Raleigh NC 27695, USA

1 Introduction

The global population was growing rapidly, with rapid increase from the 5 billion in 1987 to a staggering 7.6 billion by 2020 (World Population Statistics, US Census Bureau). Ensuring food security in a sustainable and environmentally friendly manner is the major challenge posed by large population growth, with food demand projected to increase by 70–100% (Fukase & Martin, 2020). To satisfy the demand for animal protein, pig farms continue to increase continually in both number and size. However, intensive large-scale pig farms have brought unprecedented challenges to the environment and ecosystem. In order to reduce the occurrence of livestock diseases and increase pig growth rate, various trace elements such as copper (Cu), zinc (Zn), and arsenic (As) are added to animal feed. However, due to poor metabolism, more than 90% of these additives are excreted (Li et al., 2019). Subsequent use of animal wastewater for irrigation can lead to several environmental problems, including salt toxicity to plants and accumulation of HMs in soil and contamination of groundwater (Rattan et al., 2005).

Existing heavy metal control technologies include reverse osmosis (Vaneeckhaute et al., 2019), ion exchange (Maslova et al., 2020), chemical precipitation (Baltpurvins et al., 1997; Ozverdi & Erdem, 2006), electrochemical treatment (Ya et al., 2018), etc. Despite their treatment efficiency, most of these technologies generate high levels of secondary wastes; so their effectiveness in reducing HM pollution from animal wastewater is insufficient (Kurniawan et al., 2006). The adsorption method is a promising choice for removing HMs in animal wastewater, due to its treatability, versatility, and economy (Afroze & Sen, 2018; Yin et al., 2019). Generally, adsorbents include activated carbon, zeolite, mesoporous silica, carbon nanotubes, cyclodextrin, and chitosan beads (Borji et al., 2020; Jusoh et al., 2007; Kandah & Meunier, 2007). However, these adsorbents have poor recoverability, low adsorption capacity, and lack functional structural adjustment.

In addition to possessing high adsorption efficiency and recyclability, MOFs produce less secondary waste and consume less energy than other treatment methods (Furukawa et al., 2010; Millward & Yaghi, 2005; Lu Wang et al., 2016). MOFs have shown great application potential in the field of animal wastewater treatment. Of these, zirconium-based MOF materials such as UiO-66 and its derivatives exhibit superior water and thermal stability, no toxicity, and diversity of functional group modification, which is seen as promising adsorbents for the removal of pollutants (i.e., heavy metals) in wastewater (Furukawa et al., 2014; Lv et al., 2016; Min et al., 2019). UiO-66 and its derivatives have large pore size and specific surface area, which are the key factors for their excellent adsorption performance. The hexanuclear Zr cluster nodes in their structure are suitable site for capturing anionic contaminants such as Cr (VI) and As (III)/As (V) (Shokouhfar et al., 2018). In addition, UiO-66 and its derivatives can adsorb and remove the cationic pollutants such as Hg^{2+} and Cd^{2+} under acid–base interaction and electrostatic interaction. Saleem used functionalized UiO-66-NH_2 materials as adsorbents for the capture of Cr^{3+} and Pb^{2+} from homo-ionic solution, with calculated adsorption capacities of 117 and 232 mg/g, respectively (Saleem et al., 2016). In addition, HMs such as As (Howarth et al., 2015), (Wang et al., 2015), and Sb (Luo et al., 2015) can also be effectively removed by UiO-66. Currently, most studies on the adsorption performance of UiO-66 are only based on synthetic samples, instead of real wastewater such as pig farm wastewater. Since the composition of synthetic wastewater is much simpler than the composition of the pig farm wastewater, results obtained with the synthetic wastewater may not apply in the real world. Hence, the study of heavy metal adsorption based on the complex real wastewater samples from livestock farms is very meaningful.

In this paper, octahedral UiO-66 and UiO-66-NH_2 prepared with acetic acid were used as adsorbents to selectively recover HMs from pig farm wastewater. To determine optimal treatment conditions, the influence of various reaction conditions (adsorbent dosage, pH, and adsorption time) on the adsorption efficiency of HMs was studied. Besides, the mechanism and repeatability of UiO-66 and UiO-66-NH_2 to adsorption of HMs, as well as adsorption kinetics were also studied. Based on the comparison between the Maximum Contaminant Level (MCL) of the corresponding HMs and the heavy metal residual concentration in the supernatant of adsorbent dosage, we introduced a treatability index (TI) to evaluate the

treatment effect of HMs by UiO-66 and UiO-66-NH_2 (Huang et al., 2019).

2 Materials and Methods

2.1 Chemical Reagents

Aladdin Company (Shanghai, China) supplied N'N-dimethylformamide (DMF), p-phthalic acid, 2-aminoterephthalic acid and zirconium chloride. Hydrochloric acid (HCl, 37%), acetic acid, ethanol, methanol, and sodium hydroxide were purchased from Sinopharm Chemical Reagent Co., Ltd. (China). All reagents were used without purification as received.

2.2 Materials Synthesis

The adsorbent UiO-66 was prepared following Qiu et al. (2017). Ten millimoles each of $ZrCl_4$ and terephthalic acid were dissolved in 60 mL of DMF. Thereafter, 160 mmol acetic acid was added and the solution was stirred for 2 h and ultrasonicated for 30 min. The resulting solution was heated at 120 ℃ for 24 h. After cooling, the solution was centrifuged, and the separated material was washed with DMF and ethanol. After drying and grinding, UiO-66 was obtained as a white powder. UiO-66-NH_2 was synthesized using the same procedure as UiO-66, except that terephthalic acid was replaced with 2-aminophthalic acid.

2.3 Material Characterization

The particle morphology and size of UiO-66 and UiO-66-NH_2 were observed using scanning electron microscopy (SEM; S-4800, Hitachi, Japan). X-ray diffraction (XRD) patterns of the samples were determined by the D8 Advance X-ray diffractometer (Bruker, Germany) with Cu K beam X-ray as the target in the scanning range of 5 to 90°, and the scanning speed was 3°/min. Fourier transform infrared (FT-IR) spectrum was analyzed and with the Nicolet iS10 (Thermo-fisher, USA) using KBr pressing method. Brunauer–Emmett–Teller (BET) method for specific surface area determination using N_2 adsorption was performed by using specific surface analyzer (JW-BK 100, China). Before the test, the sample was activated at 300℃ for 3 h in vacuum, and the adsorption and desorption tests were conducted using high purity liquid N_2 as adsorbate.

2.4 Adsorption Experiment

Wastewater samples were collected from a pig farm in Fenghua District, Ningbo city. The collected liquid samples were stored at 2℃. The effluent was analyzed for the constituents mentioned in Table 1. The initial pH was measured by a pH meter (Mettler FE 28, Switzerland, accuracy ± 0.01 pH units) and the dry matter content was determined by weighing difference of evaporating wastewater in an oven over night at 105 ℃ (Bourdin et al., 2014). The pH of the effluent was 8, and the dry matter content was 0.69% as shown in Table 1. Batch experiments were implemented at room temperature and designed in triplicate. In a typical study of adsorption procedure, the prepared adsorbent (0.8 g) was added to 200 mL of wastewater; this suspension was continuously stirred at a speed of 200 r/min for 270 min. At fixed intervals (10, 20, 30, 60, 90, 120, 150, 180, 210, 240, and 270 min), an aliquot (10 mL) of the supernatant was sampled, filtered (0.22 μm), and the HMs concentration in the filtrate was measured using the ICP-MS (Thermo Icap Q, USA).

To study the effect of wastewater pH, 0.8 g UiO-66 or UiO-66-NH_2 was added to 200 mL of pig farm effluent after pH adjustment using hydrochloric acid or sodium hydroxide to the desired values (pH = 2, 4, 6, 8, 10). Then, samples of the aliquots taken after 120 min were filtered and HM concentrations in the filtrate were measured. In order to investigate the influence of adsorbent dosage on HM removal, different amounts (0.4, 0.8, 1.2, 1.6, 2.0 g) of adsorbent were added to 200 mL animal wastewater at a pH of 8. For the economic and environmental reasons, we used deionized water as the washing solution for the regeneration of the adsorbents. After centrifugation and separation, the recovered adsorbents were washed three times using 20 mL ethanol. Then, the regenerated adsorbents were dried overnight and all used in a new batch of tests.

The removal rate (R, %) and adsorption capacity (Q_e, μg/g) of the adsorbent at any time (e.g., 10, 20 min) was calculated from the initial heavy metal

Table 1 The total HMs concentration in pig farm effluent (pH = 8, TS = 0.69%), their health impacts and the maximum concentration levels of those HMs in various water quality standards

HMs	Concentrations (μg/L) [a]	Impacts on human health	MCL [b]				
			Class III standards in GB 3838–2002 (μg/L) [c]	Class I standards in GB 3838–2002 (μg/L) [c]	GB 5749–2006 (μg/L) [d]	EPA (μg/L, 2016) [e]	WHO (μg/L, 2004) [f]
Cr	14.8 ± 2.4 (Total Cr)	Cause kidney and liver disease, diarrhea, ulcers, skin and eye irritation, respiratory tract irritation (Jobby et al., 2018)	50	10	50	100	50
Mn	120.5 ± 13.1	Neurologic injury, ataxia, dementia, anxiety, spasm (Lin et al., 2013)	100	100	100	50	500
Fe	3420.4 ± 595.6	-	300	300	300	300	-
Ni	70.3 ± 6.7	Vomiting, gastrointestinal diseases, nasal cavity cancer and lung cancer (Raval et al., 2016; Sarode et al., 2019)	20	20	20	-	20
Cu	369.6 ± 31.2	Lung cancer, Liver toxicity, headache, cellular damage (Anastopoulos et al., 2019; Gaetke et al., 2014)	1000	10	1000	1000	2000
Zn	1200.8 ± 110.8	Depression, lethargy, neurological symptoms and thirst (Baran et al., 2018)	1000	50	1000	5000	3000
As	25.4 ± 2.6	Nausea, vomiting, neuropathic pain, chronic conjunctivitis, shock, respiratory failure (Singh et al., 2018)	50	50	10	10	10

[a] Measurement of triplicates

[b] Maximum concentration levels of heavy metals in various standards

[c] Chinese Environmental Quality Standards for Surface Water, Class I and Class III standards

[d] Chinese domestic drinking water hygiene standards

[e] World Health Organization Drinking Water Standards

[f] National Drinking Water Regulations by U.S. Environmental Protection Agency

concentration C_0 (μg/L, t = 0) and equilibrium concentration C_e (μg/L, t = 270 min), as follows:

$$R = \left(C_0 - C_e\right)/C_0 * 100\% \quad (1)$$

$$Q_e = \left(C_0 - C_e\right) * V/m \quad (2)$$

where m (g) is the dosage of adsorbent and V (L) is solution volume.

2.5 Treatability Index

Generally, after the addition of adsorbents, the dissolved concentration of HMs decreased dramatically and then leveled off. Huang et al. (2019) compared the inflection point of the adsorption curve with the threshold value to obtain the powdered activated carbon's treatability of the pollutant. In this experiment, the residual concentration of HMs at equilibrium is close to the concentration at the inflection point of the adsorption curve. Therefore, by comparing the residual concentration of HMs in the adsorption equilibrium with the MCL according to the China Environmental Quality Standards for Surface Water (GB3838-2002) as show in Table 1, the treatability index (TI) of HMs can be calculated by the following Eq. (3):

$$TI = \left(C_T - C_e\right)/C_T \quad (3)$$

where, C_T is the MCL of the corresponding HM (μg/L). When TI is less than 0, the adsorbent cannot remove the corresponding HM (-T). When TI is greater than 0, the HM (T +) can be effectively treated by the adsorbent. The adsorbent's performance improves as the TI value approaches 1.

3 Results and Discussion

3.1 Characterization

SEM technique was used to elucidate the microstructures of UiO-66 and UiO-66-NH_2. As shown in Fig. 1a, b, these particles are uniformly distributed and highly crystalline. Their forms were regular octahedrons. The average particle sizes of UiO-66 and UiO-66-NH_2 samples are ~ 300 nm and ~ 100 nm, respectively. XRD diffraction spectrum of the samples are shown in the Fig. 1c. The results demonstrate that UiO-66 and UiO-66-NH_2 prepared by acetic acid-stimulating method have the same crystal structure as in the previously reported studies (Cavka et al., 2008; Katz et al., 2013; Lv et al., 2016). The XRD spectrum indicates that the synthesized materials have a high degree of crystallinity, as is also clear from the morphology shown in SEM images (Fig. 1a, b). Due to the enhanced crystallinity of the materials prepared in this study, the BET surface areas were 1070 and 751 m^2/g, respectively, which are higher than the reported BET surface areas of hydrochloric acid-treated UiO-66 and UiO-66-NH_2 prepared by Katz et al. (2013).

To characterize the chemical structure of adsorbents, FT-IR spectra of these sample were measured. Figure 1d shows the FT-IR spectrum, which clearly confirms the successful self-assembly of UiO-66 and UiO-66-NH_2 in the range of 3500–1000 cm^{-1}. The ligands of UiO-66 and UiO-66-NH_2 are terephthalic acid and 2-amino-terephthalic acid respectively, which are mainly composed of aromatic carboxylic acids. These peaks in the FT-IR atlas also confirm the existence of aromatic groups: 1580 cm^{-1} derived from C-O bond in carboxylate, 1500 cm^{-1} generated by aromatic group C = C, and 1420 cm^{-1} generated by C–C vibration mode (He et al., 2019; Kandiah et al., 2010). The peaks at 3448, 3368, and 1629 cm^{-1} represent symmetric, asymmetric and bending vibrations of the amino group respectively (Tang et al., 2018). C_{ar}-N corresponding to the peak at 1257 cm^{-1} also confirmed the load of amine in UiO-66-NH_2.

3.2 HM Composition and Concentration

Table 1 lists the average concentrations of the primary HMs in the pig farm effluent. Concentrations of the HMs followed a descending order of iron (Fe) > zinc (Zn) > copper (Cu) > manganese (Mn) > nickel (Ni) > arsenic (As) > cobalt (Co) > chromium (Cr). After mechanical aeration and ferric flocculant treatment, pig slurry separates into sludge and effluent. During treatment, due to adsorption and assimilation, heavy metals, microorganisms, mineral particles and inorganic salts are concentrated in the activated sludge flocs that settle down as sludge. Therefore, the concentration of HMs in pig farm effluent is much lower, by as much as 2–3 orders of magnitude than in the slurry (Tulayakul et al., 2011). The

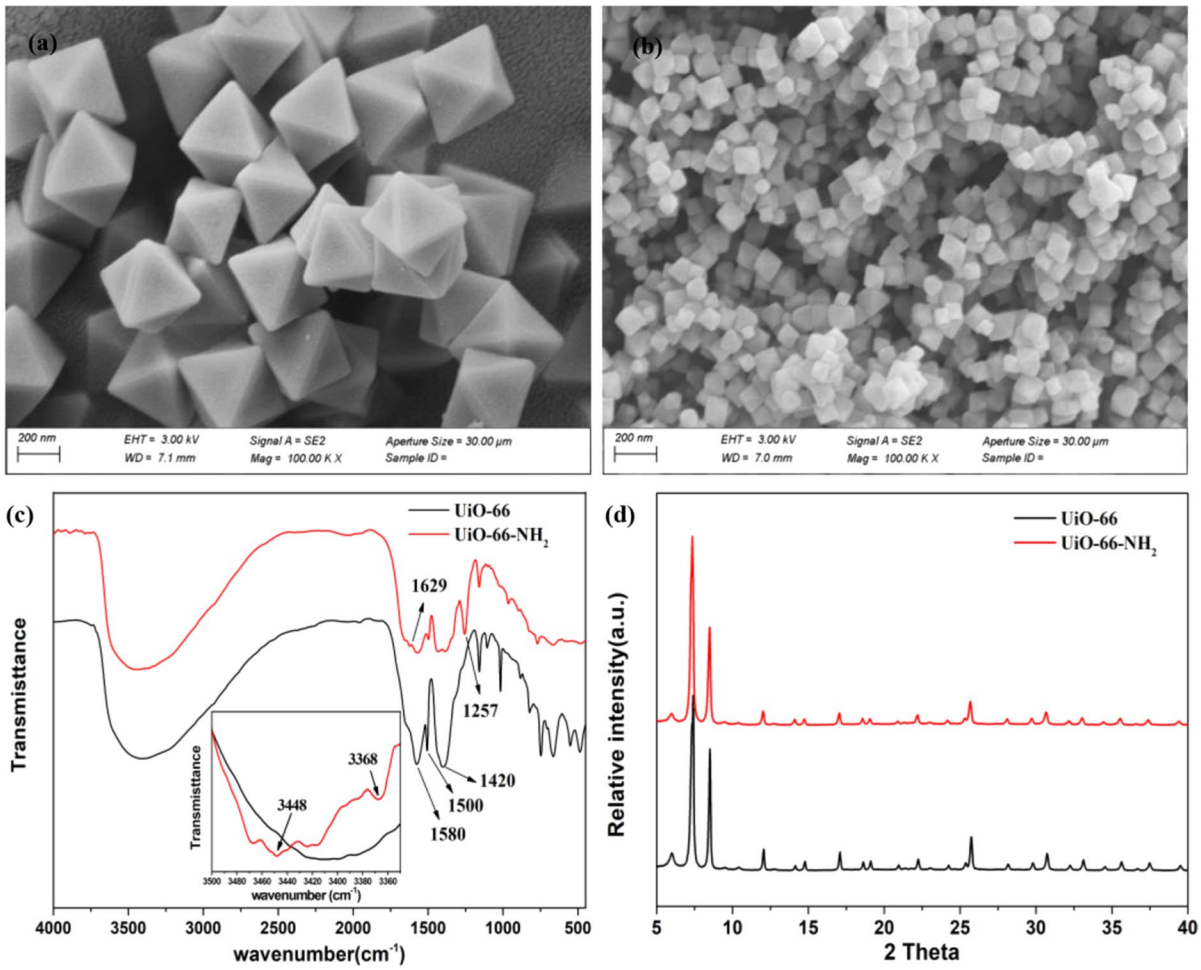

Fig. 1 The SEM images of (**a**) UiO-66 (~300 nm) and (**b**) UiO-66-NH_2 (~100 nm); the (**c**) XRD characterization and (**d**) FT-IR of UiO-66 and UiO-66-NH_2

total concentrations of Cu and Zn in this study were 369 μg/L and 1200 μg/L, respectively, which were consistent with Cu and Zn concentrations reported by Kunhikrishnan et al. (2012). The concentrations of heavy metals (i.e., Mn, Fe, Ni, and Zn) in the pig farm wastewater exceeded the limits of the class I and III Chinese Environmental Quality Standards for Surface Water (GB3838-2002), Chinese Domestic Drinking Water Hygiene Standards (GB 5749–2006), and national drinking water regulations by U.S. Environmental Protection Agency (EPA, 2016). A relatively high concentration of Fe was obtained due to the addition of iron flocculants in the wastewater treatment process. According to the standards of GB 5749–2006, WHO (2004) and EPA (2016) listed in Table 1, the concentration of As in the original samples exceeded the maximum allowable content level. The concentrations of Cr and Cu were between Class I and class III Chinese standards of environmental surface water (GB3838-2002). Therefore, it is crucial to separate HMs before effluent from animal farm is discharged into the natural environment.

3.3 Effect of Contacting Time and Adsorption Kinetics

Figure 2a, b showed the ascending curve of wastewater HMs removal efficiency as affected by the contact times with UiO-66 and UiO-66-NH_2, respectively. These curves reached their plateaus within 30 to 60 min.

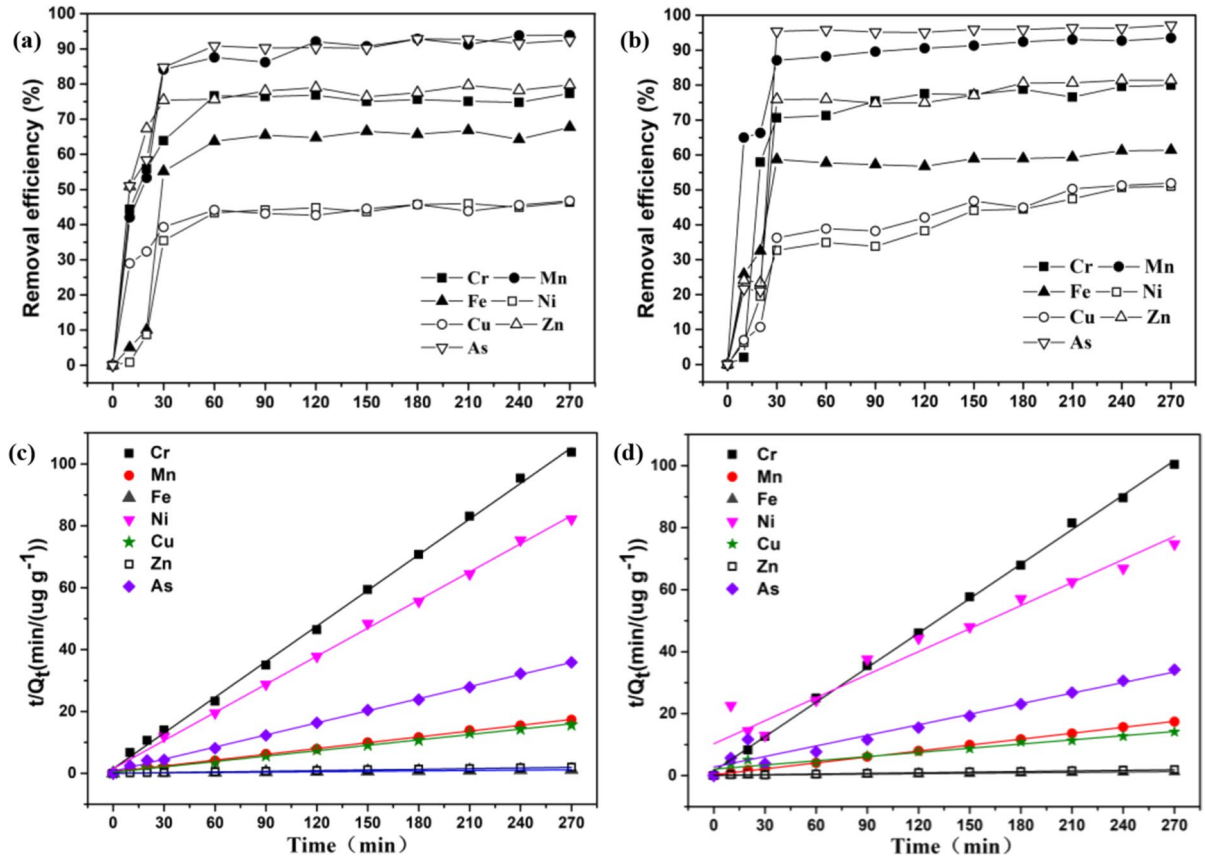

Fig. 2 Time evolution of removal efficiency during HMs adsorption on (**a**) UiO-66 and (**b**) UiO-66-NH_2; the pseudo-second-order adsorption kinetics plots of HMs on (**c**) UiO-66 and (**d**) UiO-66-NH_2. Each data point is the average of three replications

Three adsorption kinetics models were applied to study the adsorption mechanism of HMs on adsorbents. Equation (4) presents the pseudo-first-order model, which assumes the adsorption mechanism of various liquid–solid systems that adsorption increases as the dissolved concentration increases (Liying Wang et al., 2010). The pseudo-second-order model as represented by Eq. (5) assumes that the adsorption process is dominated by a chemisorption mechanism. Weber and Morris's internal diffusion dynamics model is applied to analyze the control steps in the reaction and obtain the intraparticle diffusion rate constant (k_3) of the adsorbent as presented by Eq. (6) (Malash & El-Khaiary, 2010).

$$ln\left(Q_e - Q_t\right) = lnQ_e - k_1 t \tag{4}$$

$$\frac{t}{Q_t} = \frac{t}{Q_e} + \frac{1}{K_2 Q_e^2} \tag{5}$$

$$Q_t = k_3 t^{1/2} + D \tag{6}$$

In Eq. (4), Q_e and Q_t (μg/g) are the adsorbed concentrations of contaminants at equilibrium and at any time t (min), respectively. k_1 and k_2 in Eqs. (5) and (6) are the rate constants for the adsorption kinetic model of the pseudo-first-order and pseudo-second-order, respectively. D is a constant involving thickness and boundary layer.

The HM adsorption data in pig farm the wastewater by UiO-66 showed that the pseudo-second-order fitting curves as presented in Fig. 2c described the adsorption process better. The correlation coefficient (R^2) of the pseudo-second-order adsorption model for each HM presented in Table 2S was higher than that of the pseudo-first-order model shown in Table 1S. For example, with UiO-66, the calculated adsorption capacity based on the pseudo-second-order model (2.603 μg/g) was closer to the actual

adsorption (2.601 μg/g) than the pseudo-first-order model (1.265 μg/g). The process of internal diffusion consists of mass transfer, intraparticle diffusion and adsorption equilibrium (Harja & Ciobanu, 2018). The first stage was accomplished in a short period, and so the latter two stages (intraparticle diffusion and adsorption equilibrium) were the main adsorption processes. As shown in Fig. 1S, at the beginning of the reaction, HMs were gradually adsorbed due to the existence of a large number of active sites on the surface of UiO-66. After 60 min, adsorption reached equilibrium and none of the plots passed through the origin, indicating that the internal diffusion of the particles was part of the adsorption, not the rate controlling step.

The removal rates of Cr, Mn, Zn, and As by using UiO-66-NH_2 as adsorbent showed a sharp rise during the first 20 min, and then the increase slowed until up to 150 min before it plateaued (Fig. 2b). The adsorption rates of Fe, Ni and Cu were slow in the first 20 min, and then accelerated for the next 10 min. After 30 min, the adsorption capacities of Fe, Ni, and Cu reached 205.62 μg/g, 2.31 μg/g and 13.36 μg/g, which were 95.6%, 64% and 69.8% of the maximum capacities, respectively (Fig. 2b). The equilibrium was reached after 210 min. This may be due to the special complexation of heavy metal ions with amino functionalized surface in the initial stage of the reaction, Cr, Mn, Zn, and As occupied most of the adsorption sites on UiO-66-NH_2, resulting in low removal rates of the Fe, Ni, and Cu ions. As the reaction proceeded, the concentrations of Cr, Mn, Zn, and As decreased, and the adsorption sites on the adsorbent surface became available, thereby accelerating the adsorption of Fe, Ni, and Cu on UiO-66-NH_2. Adsorption capacity reaches the maximum value as the reaction reaches the equilibrium. The maximum adsorption capacities of Cr, Mn, Fe, Ni, Cu, Zn and As by UiO-66-NH_2 were 2.69 μg/g, 15.67 μg/g, 219.78 μg/g, 4.034 μg/g, 22.22 μg/g, 153.37 μg/g, and 8.80 μg/g, respectively (Fig. 2d).

The adsorption capacity (Q_e) of Fe and Cu on UiO-66 (Fe: 237 μg/g, Cu: 17.26 μg/g) was higher than that of UiO-66-NH_2 (Fe: 215 μg/g, Cu: 3.61 μg/g), respectively, due to the higher specific surface area of the former (Table 2S). For the low concentrations of Cr, Mn, Ni, Zn, and As in the weakly alkaline pig farm wastewater, the active centers originally occupied by hydrogen ions on UiO-66-NH_2 were released, and these heavy metal ions then had opportunity to react with active centers (Tang et al., 2021). This opposing interaction is likely to be the reason causing UiO-66-NH_2 to have slightly higher Q_e for Cr, Mn, Ni, Zn and As than UiO-66.

3.4 Effect of Initial Wastewater pH

The HM adsorption capacities of UiO-66 at different pH values are shown in Fig. 3a. Depending on pH, Cr exists in the form of $HCrO_4^-$, $Cr_2O_7^{2-}$ or CrO_4^{2-}. When the wastewater is acidic, the surface charge of UiO-66 will activate the proton reaction and promote the electrostatic adsorption of Cr (Sari & Tuzen, 2008). As pH increases, the presence of OH^- competes with CrO_4^{2-}, resulting in a decrease in Cr removal rate (Fan et al., 2017). Solution pH had little effect on the removal rate of Zn by UiO-66. As pH was raised from 4 to 10, Fe removal rate declined from 94.5% to 75.8%, and the adsorption capacity decreased from 807.727 μg/g to 648.143 μg/g (Fig. 3a). The maximum removal rate and maximum adsorption capacity of Mn of 92.7% and 27.94 μg/g, respectively, was at pH of 8. The optimal pH value for As adsorption on UiO-66 is 10. At this pH, the surface charge of the material is negative and As exists in the form of almost $H_2AsO_3^-$. Therefore, the electrostatic interaction between the adsorbent and adsorbate is not the main force of the material on the adsorption of As (Shao et al., 2019).

The adsorption capacities for Cr, Fe, Ni and Cu by UiO-66-NH_2 were stronger in the alkaline range, but weaker in the acidic range (Fig. 3b). At lower pH values, free H^+ ions can compete with heavy metal ions, resulting in weakened adsorption of heavy metal ions on UiO-66-NH_2. In addition, H^+ reacts with -NH_2 and forms -NH_3^+ ions, which can further reduce HM adsorption due to coulomb repulsion between the formed -NH_3^+ and HM ions. With increase in pH value, competitive adsorption and coulomb rejection are reduced, and the adsorption of ions increases (Ding et al., 2020). Therefore, the maximum adsorption capacities for those HMs on UiO-66-NH_2 were obtained in moderately alkaline wastewaters. Hence, both UiO-66 and UiO-66-NH_2 can be used to remove common harmful HMs in animal wastewater in a wide range of pH conditions.

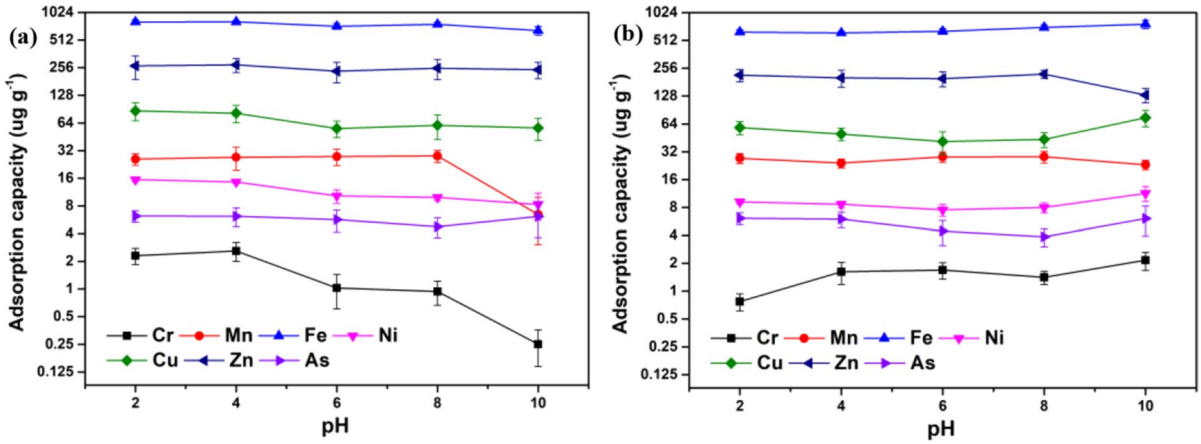

Fig. 3 Effect of pH on adsorption of HMs by (**a**) UiO-66 and (**b**) UiO-66-NH_2 (y axis values are log values). Each data point is the average of three replications and the error bars show standard deviation

3.5 Effect of Adsorbent Dosage

For practical application, from an economic perspective, the amount of adsorbent required would be very important. Figure 4 shows the plot of HM removal rate versus dosage of adsorbents. Due to increase in adsorption sites, amounts of Fe, Cu, Zn and As adsorbed increased markedly with initial adsorbent concentrations. When the initial dosage of UiO-66 was 4 g/L and pH was 8, the removal rates of Cr, Mn, Fe, Ni and As were 76.93%, 93.73%, 88.81%, 83.30% and 86.11%, respectively. At this dose, the removal rates of them by UiO-66-NH_2 were76.60%, 94.99%, 86.24%, 75.91% and 82.23%, respectively. Both of UiO-66 and UiO-66-NH_2 showed good removal effects on heavy metals at 4 g/L, which can be recommended to practical HMs treatment.

3.6 Treatability Analysis

According to the environmental protection goals, the Chinese Environmental Quality Standards for Surface Water (GB3838-2002) include five grades. As listed in Table 1, Class I standard applies mostly in

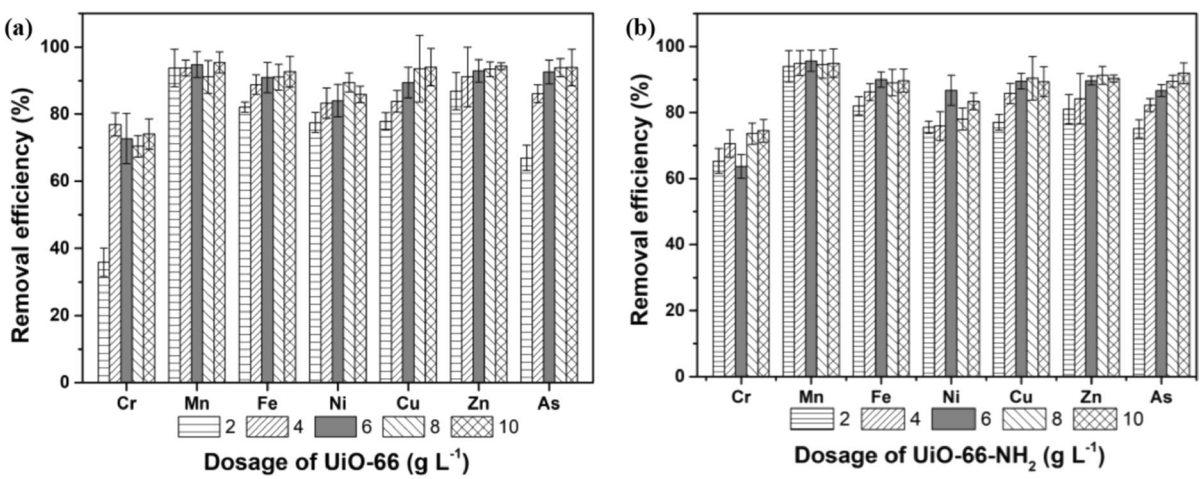

Fig. 4 Effect of initial concentration of adsorbents on adsorption of HMs by (**a**) UiO-66 and (**b**) UiO-66-NH_2. Each data point is the average of three replications and the error bars show standard deviation

source water and national nature reserves. Class III waster is mainly applicable to the secondary protection areas of centralized drinking water surface water sources, fishery water areas, aquaculture areas and swimming areas. Since many pig farms are not far from rural residential areas and locate in the suburban areas in china, Class III standards were used as the MCL value to investigate the adsorption ability of MOFs on HMs. Table 2 shows the TI values of the HMs calculated using Eq. (3). The maximum treatability index of HMs by UiO-66 treatment followed a descending order of Cu > As > Mn > Zn > Cr > Ni > Fe (dosage, 10 g/L). The TI values for Cu, As, Mn, Zn, and Cr were close to 1, which meant that at the end of the reaction, their residual concentrations were far below the threshold requirements. As the explicated by Shokouhfar et al. (2018), the adsorption process of Cr was mainly due to the hexanuclear Zr cluster (Zr_6) active sites on the structure of UiO-66 and UiO-66-NH_2 form an electrostatic interaction with Cr (VI). According to He et al. (2019), the adsorption mechanism of As (III) and As (V) by UiO-66 was mainly explained by the formation of bidentate binuclear complexes between Zr_6 and As (III), and bidentate mononuclear complexes with As (V) (He et al., 2019; Schmidt et al., 2008). Further studies on the adsorption mechanisms of individual ions, such as Cu, Mn, Ni, Fe, and Zn, are warranted on this subject.

When the dosage was 2 g/L, the TI value of Ni by UiO-66-NH_2 was 0.14, and the TI value did not increase dramatically as the dosage increasing to 10 g/L. Similar TI results of the UiO-66 on Ni adsorptions was also obtained. Therefore, increasing the dosage of UiO-66 and UiO-66-NH_2 above 6 g/L on Ni adsorption is not recommended for efficient and economical concerns. Both Zn and Fe with a relatively high initial concentrations, although the removal rate of the two ions can reach over 60% (Figs. 2 and 4), but the final TI values of Zn and Fe were 0.931 and 0.161, respectively. Except for Fe with UiO-66 at concentrations 2–8 g/L and UiO-66-NH_2 at concentration of 2–10 g/L, TIs for all other combinations of adsorbent concentrations and types were > 0 (Table 2), which means the residual concentration of Fe was higher than the threshold, and the treatment effect cannot meet the standard requirements. To better understand the adsorption ability and the mechanisms of the adsorption, further studies on the adsorption mechanisms of individual ions (i.e., such as Cu, Mn, Ni, and Fe) as well as the ions adsorption interaction mechanisms in a complex wastewater system are needed due to the lack of related information in present.

3.7 Regeneration and Reuse of Adsorbents

The techno-economic efficacy of MOFs is related to its reusability after multiple adsorption cycles. Figure 5 showed the reuse efficiency of adsorbents after three cycles of regeneration. After three adsorption treatment cycle, the HMs average removal efficiency by UiO-66 and UiO-66-NH_2 of the third time was reduced by only 11.5% and 12.8%, respectively, compared to the first time. In order to analyze the difference in the adsorption effect of the two materials, T-test was performed on the adsorption capacity of the two adsorbents. As shown in Table 3S, the adsorption capacity of UiO-66 for Mn and Zn is significantly higher than that of UiO-66-NH_2 ($P < 0.05$) after three cycles. For Cr, Ni, Cu and As, the difference of adsorption performance between the two adsorbents is negligible. The result shows that the adsorbents can be regenerated and reused multiple times, but there is still space for improvement. New studies on the regeneration procedures using organic washing solvents are suggested for improving the reusability of the adsorbents (Esrafili et al., 2021). The adsorbent recovery technology of centrifugation used in small-scale experiments will bring economic burden in practical applications, therefore, economic and environmentally friendly recovery technology still needs to be investigated in future works.

In this study, all materials were successfully prepared by solvothermal method during the laboratory-scale investigation. In the subsequent large-scale applications, the existing preparation method such as organic solvent-based system can be replaced by the aqueous-based preparation system, which may reduce the cost to 14.2 ~ 17.5 $/kg while improving production efficiency (Luo et al., 2021). Therefore, considering the adsorption capacity, recycling ability, secondary pollution to the environment and economy of the material, UiO-66-based MOFs can indeed be used as a new adsorbent for the treatment of heavy metals in wastewater.

Table 2 Treatability of the 7 HMs by UiO-66 and UiO-66-NH_2

Elements	MCL [a]	Dosage (g/L)	UiO-66			UiO-66-NH_2		
			Residual concentration (μg/L) [b]	TI [c]	Treatability [d]	Residual concentration (μg/L) [b]	TI [c]	Treatability [d]
Cr	50	2	9.52	0.810	**T +**	5.15	0.897	**T +**
		4	3.43	0.931	**T +**	4.37	0.913	**T +**
		6	4.05	0.919	**T +**	5.40	0.892	**T +**
		8	4.39	0.912	**T +**	3.92	0.922	**T +**
		10	3.85	0.923	**T +**	3.79	0.924	**T +**
Mn	100	2	7.53	0.925	**T +**	7.19	0.928	**T +**
		4	7.55	0.924	**T +**	6.04	0.940	**T +**
		6	6.32	0.937	**T +**	5.21	0.948	**T +**
		8	10.74	0.893	**T +**	6.51	0.935	**T +**
		10	5.53	0.945	**T +**	6.03	0.940	**T +**
Fe	300	2	612.74	−1.042	**−T**	615.98	−1.053	**−T**
		4	382.83	−0.276	**−T**	470.55	−0.568	**−T**
		6	310.51	−0.035	**−T**	342.18	−0.141	**−T**
		8	306.08	−0.020	**−T**	374.30	−0.248	**−T**
		10	251.68	0.161	**T +**	352.94	−0.176	**−T**
Ni	20	2	15.82	0.209	**T +**	17.19	0.140	**T +**
		4	11.73	0.413	**T +**	16.92	0.154	**T +**
		6	11.21	0.440	**T +**	9.32	0.534	**T +**
		8	7.43	0.628	**T +**	15.43	0.228	**T +**
		10	9.91	0.505	**T +**	11.66	0.417	**T +**
Cu	1000	2	81.90	0.918	**T +**	84.89	0.915	**T +**
		4	59.74	0.940	**T +**	52.54	0.947	**T +**
		6	39.09	0.961	**T +**	38.69	0.961	**T +**
		8	23.83	0.976	**T +**	35.45	0.965	**T +**
		10	22.11	0.978	**T +**	39.28	0.961	**T +**
Zn	1000	2	158.19	0.842	**T +**	227.79	0.772	**T +**
		4	106.95	0.893	**T +**	189.80	0.810	**T +**
		6	85.29	0.915	**T +**	123.75	0.876	**T +**
		8	79.46	0.921	**T +**	104.86	0.895	**T +**
		10	68.56	0.931	**T +**	115.95	0.884	**T +**
As	50	2	8.39	0.832	**T +**	6.32	0.874	**T +**
		4	3.53	0.929	**T +**	4.52	0.910	**T +**
		6	1.89	0.962	**T +**	3.39	0.932	**T +**
		8	1.56	0.969	**T +**	2.67	0.947	**T +**
		10	1.55	0.969	**T +**	2.05	0.959	**T +**

[a] Maximum concentration levels of heavy metals in the China Environmental Quality Standards in the Surface Water, Class I and III standards

[b] Concentrations of heavy metals in the adsorption equilibrium (t = 270 min)

[c] Values were calculated according to Eq. (3)

[d] ***T+***, Can be effectively processed; **−*T***, Can't be effectively processed

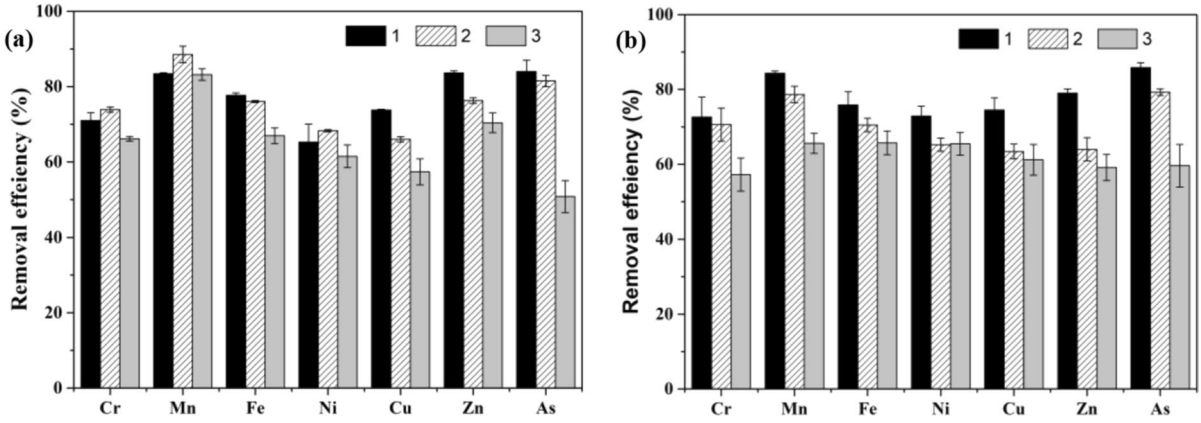

Fig. 5 Reusability of UiO-66 (**a**) and UiO-66-NH_2 (**b**) for the adsorption of HMs. Each data point is the average of three replications and the error bars show standard deviation

4 Conclusion

Octahedral UiO-66 and UiO-66-NH_2 adsorbents with large surface areas were successfully synthesized by an acid promoted solvothermal method. They have high adsorption capacity and adsorption stability, and both adsorbents removed HMs from pig farm wastewater effectively. The pseudo-second-order model accurately described the kinetic adsorption of HMs in wastewater by UiO-66 and UiO-66-NH_2 process. The treatability of 7 HMs by UiO-66 and UiO-66-NH_2 has been evaluated in this study. A novel method, established based on the equilibrium concentration of the residual heavy metals and the MCL, was used to be assess the treatability of heavy metals by UiO-66 and UiO-66-NH_2. The results show that Cu, As, Mn, Zn, Cr, and Ni can be effectively removed by the two adsorbents at the dosage of 2 g/L. Except that Fe cannot be effectively removed, which is due to the excessively high initial concentration of Fe and the lower treatment effect of these two adsorbents. UiO-66 and UiO-66-NH_2 can be reused when adsorbing HMs in wastewater and have a good adsorption performance after 3 regeneration cycles. Therefore, these MOFs showed practical applied value in the treatment of HMs in animal wastewater.

Supplementary Information The online version contains supplementary material available at https://doi.org/10.1007/s11270-021-05229-6.

Author Contribution X. Dai (Research associate) designed the experiment, wrote and edited the manuscript. L. Wang (M.S. student) and Z. Man (Ph.D. student) performed the experiment, drafted and revised the manuscript. J. Li. (Associate Researcher) supervised on the materials synthesis. Y. Jiang (Associate professor), D. Liu (Researcher) and H. Xiao (Researcher) provided research ideas and edited the manuscript. S. Shah (Professor) provided intellectual contribution to improving the manuscript.

Funding This study was funded by the Ningbo Science and Technology Bureau Public Welfare Program (2019C10076), and the National Science Foundation for Young Scientists of China (41605094).

Data Availability Available.

Code Availability Not applicable.

Declarations

Conflict of Interest The authors declare no competing interests.

References

Afroze, S., & Sen, T. K. (2018). A review on heavy metal ions and dye adsorption from water by agricultural solid waste adsorbents. *Water Air and Soil Pollution, 229*(7),https://doi.org/10.1007/s11270-018-3869-z.

Anastopoulos, I., Pashalidis, I., Hosseini-Bandegharaei, A., Giannakoudakis, D. A., Robalds, A., Usman, M., et al. (2019). Agricultural biomass/waste as adsorbents for toxic metal decontamination of aqueous solutions. *Journal of*

Molecular Liquids, 295.https://doi.org/10.1016/j.molliq.2019.111684.

Baltpurvins, K. A., Burns, R. C., Lawrance, G. A., & Stuart, A. D. (1997). Effect of electrolyte composition on zinc hydroxide precipitation by lime. *Water Research, 31*(5), 973–980. https://doi.org/10.1016/s0043-1354(96)00327-2.

Baran, A., Wieczorek, J., Mazurek, R., Urbanski, K., & Klimkowicz-Pawlas, A. (2018). Potential ecological risk assessment and predicting zinc accumulation in soils. *Environmental Geochemistry and Health, 40*(1), 435–450. https://doi.org/10.1007/s10653-017-9924-7.

Borji, H., Ayoub, G. M., Bilbeisi, R., Nassar, N., & Malaeb, L. (2020). How effective are nanomaterials for the removal of heavy metals from water and wastewater? *Water Air and Soil Pollution, 231*(7).https://doi.org/10.1007/s11270-020-04681-0.

Bourdin, F., Sakrabani, R., Kibblewhite, M. G., & Lanigan, G. J. (2014). Effect of slurry dry matter content, application technique and timing on emissions of ammonia and greenhouse gas from cattle slurry applied to grassland soils in Ireland. *Agriculture Ecosystems & Environment, 188*, 122–133. https://doi.org/10.1016/j.agee.2014.02.025.

Cavka, J. H., Jakobsen, S., Olsbye, U., Guillou, N., Lamberti, C., Bordiga, S., et al. (2008). A new zirconium inorganic building brick forming metal organic frameworks with exceptional stability. *Journal of the American Chemical Society, 130*(42), 13850–13851. https://doi.org/10.1021/ja8057953.

Ding, L., Shao, P., Luo, Y., Yin, X., Yu, S., Fang, L., et al. (2020). Functionalization of UiO-66-NH_2 with rhodanine via amidation: Towarding a robust adsorbent with dual coordination sites for selective capture of Ag(I) from wastewater. *Chemical Engineering Journal, 382*,https://doi.org/10.1016/j.cej.2019.123009.

EPA (2016). National Primary Drinking Water Regulations. https://www.epa.gov/sites/production/files/2016-06/documents/npwdr_complete_table.pdf. Accessed June 2016

Esrafili, L., Firuzabadi, F. D., Morsali, A., & Hu, M.-L. (2021). Reuse of predesigned dual-functional metal organic frameworks (DF-MOFs) after heavy metal removal. *Journal of Hazardous Materials, 403*, 123696. https://doi.org/10.1016/j.jhazmat.2020.123696.

Fan, S., Wang, Y., Li, Y., Tang, J., Wang, Z., Tang, J., et al. (2017). Facile synthesis of tea waste/Fe_3O_4 nanoparticle composite for hexavalent chromium removal from aqueous solution. *Rsc Advances, 7*(13), 7576–7590. https://doi.org/10.1039/c6ra27781k.

Fukase, E., & Martin, W. (2020). Economic growth, convergence, and world food demand and supply. *World Development, 132*, 4954–4954.

Furukawa, H., Gandara, F., Zhang, Y.-B., Jiang, J., Queen, W. L., Hudson, M. R., et al. (2014). Water adsorption in porous metal-organic frameworks and related materials. *Journal of the American Chemical Society, 136*(11), 4369–4381. https://doi.org/10.1021/ja500330a.

Furukawa, H., Ko, N., Go, Y. B., Aratani, N., Choi, S. B., Choi, E., et al. (2010). Ultrahigh porosity in metal-organic frameworks. *Science, 329*(5990), 424–428. https://doi.org/10.1126/science.1192160.

Gaetke, L. M., Chow-Johnson, H. S., & Chow, C. K. (2014). Copper: Toxicological relevance and mechanisms. *Archives of Toxicology, 88*(11), 1929–1938. https://doi.org/10.1007/s00204-014-1355-y.

Harja, M., & Ciobanu, G. (2018). Studies on adsorption of oxytetracycline from aqueous solutions onto hydroxyapatite. *Science of the Total Environment, 628–629*, 36–43. https://doi.org/10.1016/j.scitotenv.2018.02.027.

He, X., Deng, F., Shen, T., Yang, L., Chen, D., Luo, J., et al. (2019). Exceptional adsorption of arsenic by zirconium metal-organic frameworks: Engineering exploration and mechanism insight. *Journal of Colloid and Interface Science, 539*, 223–234. https://doi.org/10.1016/j.jcis.2018.12.065.

Howarth, A. J., Katz, M. J., Wang, T. C., Platero-Prats, A. E., Chapman, K. W., Hupp, J. T., et al. (2015). High efficiency adsorption and removal of selenate and selenite from water using metal-organic frameworks. *Journal of the American Chemical Society, 137*(23), 7488–7494. https://doi.org/10.1021/jacs.5b03904.

Huang, X., Lu, Q., Hao, H., Wei, Q., Shi, B., Yu, J., et al. (2019). Evaluation of the treatability of various odor compounds by powdered activated carbon. *Water Research, 156*, 414–424. https://doi.org/10.1016/j.watres.2019.03.043.

Jobby, R., Jha, P., Yadav, A. K., & Desai, N. (2018). Biosorption and biotransformation of hexavalent chromium Cr(VI): A comprehensive review. *Chemosphere, 207*, 255–266. https://doi.org/10.1016/j.chemosphere.2018.05.050.

Jusoh, A., Shiung, L. S., Ali, N., & Noor, M. J. M. M. (2007). A simulation study of the removal efficiency of granular activated carbon on cadmium and lead. *Desalination, 206*(1–3), 9–16. https://doi.org/10.1016/j.desal.2006.04.048.

Kandah, M. I., & Meunier, J.-L. (2007). Removal of nickel ions from water by multi-walled carbon nanotubes. *Journal of Hazardous Materials, 146*(1–2), 283–288. https://doi.org/10.1016/j.jhazmat.2006.12.019.

Kandiah, M., Usseglio, S., Svelle, S., Olsbye, U., Lillerud, K. P., & Tilset, M. (2010). Post-synthetic modification of the metal-organic framework compound UiO-66. *Journal of Materials Chemistry, 20*(44), 9848–9851. https://doi.org/10.1039/c0jm02416c.

Katz, M. J., Brown, Z. J., Colon, Y. J., Siu, P. W., Scheidt, K. A., Snurr, R. Q., et al. (2013). A facile synthesis of UiO-66, UiO-67 and their derivatives. *Chemical Communications, 49*(82), 9449–9451. https://doi.org/10.1039/c3cc46105j.

Kunhikrishnan, A., Bolan, N. S., Mueller, K., Laurenson, S., Naidu, R., & Kim, W.-I. (2012). The influence of wastewater irrigation on the transformation and bioavailability of heavy metal (loid)s in soil. In D. L. Sparks (Ed.), *Advances in Agronomy, Vol 115* (Vol. 115, pp. 215–297, Advances in Agronomy).

Kurniawan, T. A., Chan, G. Y. S., Lo, W. H., & Babel, S. (2006). Physico-chemical treatment techniques for wastewater laden with heavy metals. *Chemical Engineering Journal, 118*(1–2), 83–98. https://doi.org/10.1016/j.cej.2006.01.015.

Li, J., Xu, Y., Wang, L., & Li, F. (2019). Heavy metal occurrence and risk assessment in dairy feeds and manures from the typical intensive dairy farms in China. *Environmental Science and Pollution Research, 26*(7), 6348–6358. https://doi.org/10.1007/s11356-019-04125-1.

Lin, J.-L., Huang, C., Ruhsing, P. J., & Wang, Y.-S. (2013). Fouling mitigation of a dead-end microfiltration by mixing-enhanced preoxidation for Fe and Mn removal from groundwater. *Colloids and Surfaces a-Physicochemical and Engineering Aspects, 419*, 87–93. https://doi.org/10.1016/j.colsurfa.2012.11.053.

Luo, H., Cheng, F., Huelsenbeck, L., & Smith, N. (2021). Comparison between conventional solvothermal and aqueous solution-based production of UiO-66-NH_2: Life cycle assessment, techno-economic assessment, and implications for CO_2 capture and storage. *Journal of Environmental Chemical Engineering, 9*(2), 105159. https://doi.org/10.1016/j.jece.2021.105159.

Luo, J., Luo, X., Crittenden, J., Qu, J., Bai, Y., Peng, Y., et al. (2015). Removal of antimonite (Sb(III)) and antimonate (Sb(V)) from aqueous solution using carbon nanofibers that are decorated with zirconium oxide (ZrO_2). *Environmental Science & Technology, 49*(18), 11115–11124. https://doi.org/10.1021/acs.est.5b02903.

Lv, G., Liu, J., Xiong, Z., Zhang, Z., & Guan, Z. (2016). Selectivity adsorptive mechanism of different nitrophenols on UIO-66 and UIO-66-NH_2 in aqueous solution. *Journal of Chemical and Engineering Data, 61*(11), 3868–3876. https://doi.org/10.1021/acs.jced.6b00581.

Malash, G. F., & El-Khaiary, M. I. (2010). Piecewise linear regression: A statistical method for the analysis of experimental adsorption data by the intraparticle-diffusion models. *Chemical Engineering Journal, 163*(3), 256–263. https://doi.org/10.1016/j.cej.2010.07.059.

Maslova, M., Ivanenko, V., Yanicheva, N., & Gerasimova, L. (2020). The effect of heavy metal ions hydration on their sorption by a mesoporous titanium phosphate ion-exchanger. *Journal of Water Process Engineering, 35*,https://doi.org/10.1016/j.jwpe.2020.101233.

Millward, A. R., & Yaghi, O. M. (2005). Metal-organic frameworks with exceptionally high capacity for storage of carbon dioxide at room temperature. *Journal of the American Chemical Society, 127*(51), 17998–17999. https://doi.org/10.1021/ja0570032.

Min, X., Wu, X., Shao, P., Ren, Z., Ding, L., & Luo, X. (2019). Ultra-high capacity of lanthanum-doped UiO-66 for phosphate capture: Unusual doping of lanthanum by the reduction of coordination number. *Chemical Engineering Journal, 358*, 321–330. https://doi.org/10.1016/j.cej.2018.10.043.

Ozverdi, A., & Erdem, M. (2006). Cu^{2+}, Cd^{2+} and Pb^{2+} adsorption from aqueous solutions by pyrite and synthetic iron sulphide. *Journal of Hazardous Materials, 137*(1), 626–632. https://doi.org/10.1016/j.jhazmat.2006.02.051.

Qiu, J., Feng, Y., Zhang, X., Jia, M., & Yao, J. (2017). Acid-promoted synthesis of UiO-66 for highly selective adsorption of anionic dyes: Adsorption performance and mechanisms. *Journal of Colloid and Interface Science, 499*, 151–158. https://doi.org/10.1016/j.jcis.2017.03.101.

Rattan, R. K., Datta, S. P., Chhonkar, P. K., Suribabu, K., & Singh, A. K. (2005). Long-term impact of irrigation with sewage effluents on heavy metal content in soils, crops and groundwater — A case study. *Agriculture Ecosystems & Environment, 109*(3–4), 310–322. https://doi.org/10.1016/j.agee.2005.02.025.

Raval, N. P., Shah, P. U., & Shah, N. K. (2016). Adsorptive removal of nickel(II) ions from aqueous environment: A review. *Journal of Environmental Management, 179*, 1–20. https://doi.org/10.1016/j.jenvman.2016.04.045.

Saleem, H., Rafique, U., & Davies, R. P. (2016). Investigations on post-synthetically modified UiO-66-NH_2 for the adsorptive removal of heavy metal ions from aqueous solution. *Microporous and Mesoporous Materials, 221*, 238–244. https://doi.org/10.1016/j.micromeso.2015.09.043.

Sari, A., & Tuzen, M. (2008). Biosorption of total chromium from aqueous solution by red algae (Ceramium virgatum): Equilibrium, kinetic and thermodynamic studies. *Journal of Hazardous Materials, 160*(2–3), 349–355. https://doi.org/10.1016/j.jhazmat.2008.03.005.

Sarode, S., Upadhyay, P., Khosa, M. A., Mak, T., Shakir, A., Song, S., et al. (2019). Overview of wastewater treatment methods with special focus on biopolymer chitin-chitosan. *International Journal of Biological Macromolecules, 121*, 1086–1100. https://doi.org/10.1016/j.ijbiomac.2018.10.089.

Schmidt, G. T., Vlasova, N., Zuzaan, D., Kersten, M., & Daus, B. (2008). Adsorption mechanism of arsenate by zirconyl-functionalized activated carbon. *Journal of Colloid and Interface Science, 317*(1), 228–234. https://doi.org/10.1016/j.jcis.2007.09.012.

Shao, P., Ding, L., Luo, J., Luo, Y., You, D., Zhang, Q., et al. (2019). Lattice-defect-enhanced adsorption of arsenic on zirconia nanospheres: A combined experimental and theoretical study. *Acs Applied Materials & Interfaces, 11*(33), 29736–29745. https://doi.org/10.1021/acsami.9b06041.

Shokouhfar, N., Aboutorabi, L., & Morsali, A. (2018). Improving the capability of UiO-66 for Cr(VI) adsorption from aqueous solutions by introducing isonicotinate N-oxide as the functional group. *Dalton Transactions, 47*(41), 14549–14555. https://doi.org/10.1039/c8dt03196g.

Singh, C. K., Kumar, A., & Bindal, S. (2018). Arsenic contamination in Rapti River Basin, Terai region of India. *Journal of Geochemical Exploration, 192*, 120–131. https://doi.org/10.1016/j.gexplo.2018.06.010.

Tang, J., Chen, Y., Zhao, M., Wang, S., & Zhang, L. (2021). Phenylthiosemicarbazide-functionalized UiO-66-NH_2 as highly efficient adsorbent for the selective removal of lead from aqueous solutions. *Journal of Hazardous Materials, 413*,https://doi.org/10.1016/j.jhazmat.2021.125278.

Tang, P., Wang, R., & Chen, Z. (2018). In situ growth of Zr-based metal-organic framework UiO-66-NH_2 for open-tubular capillary electrochromatography. *Electrophoresis, 39*(20), 2619–2625. https://doi.org/10.1002/elps.201800057.

Tulayakul, P., Boonsoongnern, A., Kasemsuwan, S., Wiriyarampa, S., Pankumnoed, J., Tippayaluck, S., et al. (2011). Comparative study of heavy metal and pathogenic bacterial contamination in sludge and manure in biogas and non-biogas swine farms. *Journal of Environmental Sciences, 23*(6), 991–997. https://doi.org/10.1016/s1001-0742(10)60484-6.

Vaneeckhaute, C., Darveau, O., & Meers, E. (2019). Fate of micronutrients and heavy metals in digestate processing using vibrating reversed osmosis as resource recovery

technology. *Separation and Purification Technology, 223*, 81–87. https://doi.org/10.1016/j.seppur.2019.04.055.

Wang, C., Liu, X., Chen, J. P., & Li, K. (2015). Superior removal of arsenic from water with zirconium metal-organic framework UiO-66. *Scientific Reports, 5*, https://doi.org/10.1038/srep16613.

Wang, L., Han, Y., Feng, X., Zhou, J., Qi, P., & Wang, B. (2016). Metal-organic frameworks for energy storage: Batteries and supercapacitors. *Coordination Chemistry Reviews, 307*, 361–381. https://doi.org/10.1016/j.ccr.2015.09.002.

Wang, L., Sun, Y., Wang, J., Wang, J., Yu, A., Zhang, H., et al. (2010). Water-soluble ZnO-Au nanocomposite-based probe for enhanced protein detection in a SPR biosensor system. *Journal of Colloid and Interface Science, 351*(2), 392–397. https://doi.org/10.1016/j.jcis.2010.07.050.

WHO (2004). Guidelines for Drinking Water Quality (third ed.), vol. 1, WHO, Geneva (2004) Recommendations. http://www.who.int/iris/handle/10665/42852. Accessed May 2004

Ya, V., Martin, N., Chou, Y.-H., Chen, Y.-M., Choo, K.-H., Chen, S.-S., et al. (2018). Electrochemical treatment for simultaneous removal of heavy metals and organics from surface finishing wastewater using sacrificial iron anode. *Journal of the Taiwan Institute of Chemical Engineers, 83*, 107–114. https://doi.org/10.1016/j.jtice.2017.12.004.

Yin, X., Shao, P., Ding, L., Xi, Y., Zhang, K., Yang, L., et al. (2019). Protonation of rhodanine polymers for enhancing the capture and recovery of Ag^+ from highly acidic wastewater. *Environmental Science-Nano, 6*(11), 3307–3315. https://doi.org/10.1039/c9en00833k.